

A Novel Dynamic Quadrature Scheme for Solving Boltzmann Equation with Discrete Ordinate and Lattice Boltzmann Methods

C. T. Hsu*, S. W. Chiang and K. F. Sin

Department of Mechanical Engineering, Hong Kong University of Science and Technology, Clear Water Bay, Kowloon, Hong Kong.

Received 15 May 2010; Accepted (in revised version) 15 May 2011

Available online 30 November 2011

Abstract. The Boltzmann equation (BE) for gas flows is a time-dependent nonlinear differential-integral equation in 6 dimensions. The current simplified practice is to linearize the collision integral in BE by the BGK model using Maxwellian equilibrium distribution and to approximate the moment integrals by the discrete ordinate method (DOM) using a finite set of velocity quadrature points. Such simplification reduces the dimensions from 6 to 3, and leads to a set of linearized discrete BEs. The main difficulty of the currently used (conventional) numerical procedures occurs when the mean velocity and the variation of temperature are large that requires an extremely large number of quadrature points. In this paper, a novel dynamic scheme that requires only a small number of quadrature points is proposed. This is achieved by a velocity-coordinate transformation consisting of Galilean translation and thermal normalization so that the transformed velocity space is independent of mean velocity and temperature. This enables the efficient implementation of Gaussian-Hermite quadrature. The velocity quadrature points in the new velocity space are fixed while the correspondent quadrature points in the physical space change from time to time and from position to position. By this dynamic nature in the physical space, this new quadrature scheme is termed as the dynamic quadrature scheme (DQS). The DQS was implemented to the DOM and the lattice Boltzmann method (LBM). These new methods with DQS are therefore termed as the dynamic discrete ordinate method (DDOM) and the dynamic lattice Boltzmann method (DLBM), respectively. The new DDOM and DLBM have been tested and validated with several testing problems. Of the same accuracy in numerical results, the proposed schemes are much faster than the conventional schemes. Furthermore, the new DLBM have effectively removed the incompressible and isothermal restrictions encountered by the conventional LBM.

AMS subject classifications: 35Q20, 76N15

Key words: Dynamics quadrature, dynamic discrete ordinate method, dynamic lattice Boltzmann method, thermal lattice Boltzmann method.

*Corresponding author. *Email addresses:* mecthsu@ust.hk (C. T. Hsu), ben.chiang@family.ust.hk (S. W. Chiang), meskf@ust.hk (K. F. Sin)

1 Introduction

It has been well established that gas flows can be described by the Boltzmann equation (BE) derived from statistical mechanics based on kinetic theory of molecules. However, the Boltzmann equation is a time-dependent nonlinear differential-integral equation in 6 dimensions whose solution is very complicated, difficult and rare. The currently more simplified approach is to linearize the collision integral in BE by the BGK model with an equilibrium Maxwellian distribution and to approximate the moment integrals by the discrete ordinate method (DOM) [1–4] using a finite set of velocity quadrature points. This reduces the dimensions of BE from 6 to 3, and leads to a finite set of linearized Boltzmann equations which can be solved numerically.

The discrete ordinate method (DOM), that had been used long to solve Boltzmann equation for gas flows, was pioneered by Broadwell [1, 2] who employed a very small set of discrete velocities but was able to produce shocks. With the increase in computing power of computer in the last two decades, the DOM has attracted great attention for solving the Boltzmann equation using a large number of discrete velocities. All these early treatments made use of discretization with quadrature points in the velocity space to construct a discrete collision mechanism on the each grid node [5, 6]. A quadrature using fixed velocity points in real physical space to approximate integrals could not be implemented efficiently for obtaining hydrodynamic moments, particularly for high Mach number flows. The difficulty stems from the fact that the accurate integration of Maxwellian distribution depends highly on the temperature and the mean velocity. This requires the use of large number of quadrature points to maintain the integration accuracy when Mach number is high. As a result, huge computational resources are required to capture the flow characteristics.

In this paper, a dynamic quadrature scheme (DQS) for DOM that requires only small quadrature points to approximate accurately the moments of velocity distribution function is proposed. This is achieved through a velocity-coordinate transformation featured with Galilean translation and thermal normalization. The transformation renders the normalized Maxwellian equilibrium distribution with directional isotropy and spatial homogeneity, which enable the accurate and efficient implementation of the Gaussian-Hermite quadrature. The velocity quadrature points in the transformed velocity space are fixed while the correspondent velocity quadrature points in the physical space change from time to time and from position to position. By this dynamic nature in the physical space, we term this new scheme as the dynamic quadrature scheme (DQS). A discrete ordinate method (DOM) with the DQS is then termed as the dynamic discrete ordinate method (DDOM).

Lattice Boltzmann method (LBM), which had been developed for decades, is also a popular and powerful numerical tool to solve the Boltzmann equation for gas flows [7–10]. The LBM also uses discrete velocity set as the DOM used, except that discrete velocities in LBM are specifically assigned to ensure that a particle leaves one lattice node always resides on another lattice node. Hence the LBM can be regarded as a subset of

DOM. With the simplicity of algorithm that can reasonably capture the physics of Boltzmann equation, the LBM was used widely and indistinguishably to study many classical fluid problems [11]. It was also used as a favourable platform for designing algorithm to tackle multi-physics problems. Nevertheless, the currently-used (conventional) LBM has its limitation in solving the BE. The efficient implementation of LBM requires that the discrete velocities be isotropic and that the lattice nodes be homogeneous. These requirements restrict the applications of the conventional LBM schemes to incompressible and isothermal flows. Such restrictions defy the original physics of Boltzmann equation. In the past decades, considerable efforts have been devoted to the development of thermally enabled LBM [12]. Different kinds of thermal LBM had been proposed, but they are of less satisfactory due to various deficiencies, such as non-Galilean invariance and instabilities inherited in the thermal scheme [13]. Much effort has been devoted to the removal of these incompressible and isothermal restrictions, but of less success.

In this study, by implementing the DQS, a novel dynamic lattice Boltzmann method (DLBM) that is free of the incompressible and isothermal restrictions is proposed. This requires the transformation of the six dimensional phase space in both geometry and velocity. The transformed Boltzmann equation contains additional terms due to local convection and acceleration. The LBM with the DQS is then named as the dynamic lattice Boltzmann method (DLBM). The transformed Boltzmann equations are then solved numerically in the new coordinate system with the fixed quadrature points.

To demonstrate and validate the above new schemes, both DDOM and DLBM are tested with benchmark problems. The DDOM is tested and evaluated with 1-D Sod problems, 2-D Riemann problems and 2-D backward-step problems, incorporated with the numerical schemes used in the conventional DOM. The results indicate that the convergence rate of DDOM with the non-dimensional DQS is much faster than that of the conventional DOM with dimensional quadrature. This is mainly due to the much smaller number of quadrature points is needed for DDOM than that for DOM. Moreover, the convergence rate of DDOM is insensitive to the mean velocity and temperature. Comparison of results of DDOM for the 2-D Riemann problem with those of conventional DOM shows a good agreement. At the same degree of numerical accuracy, it is demonstrated that for the 2-D problems the DDOM can achieve a speed-up of 20-times faster than conventional DOM of the same computational efficiency, as a result of the much less quadrature points needed for DDOM than for conventional DOM, particularly at high Mach number.

Validations of the DLBM have been carried out with a 3-D numerical code for the benchmark problem of thermal instability of Rayleigh-Benard convection (RBC). The DLBM numerical solutions for the cases of Rayleigh number at 1800 and 4000 illustrate the onset of 2-D vortex rolls and 3-D hexagonal cells, respectively. The simulated results of the RBC flows are in excellent agreement with those predicted from theory, and with those obtained from the traditional macroscopic NSF equations. Apparently, the new DLBM has basically removed the incompressible and isothermal restrictions associated with the conventional LBM. On the DLBM we did not experience the numerical instability as encountered on the conventional LBM for thermal flow problem. It is conceived

that this numerical instability may have been due to the small Mach number expansion employed in the conventional LBM.

2 Boltzmann equation with BGK collision model for gas flows

The Boltzmann equation (BE), derived from statistical mechanics based on gas kinetic theory, describes the evolution of the velocity distribution function $f(\mathbf{r}, \mathbf{c}, t)$ of dilute gases of identical molecules in the phase space. The equation is a time-dependent nonlinear differential-integral equation in phase space of 6 dimensions. After the linearization of its collision integral with the BGK model, the BE is given by

$$\frac{\partial f}{\partial t} + \mathbf{c} \cdot \frac{\partial f}{\partial \mathbf{r}} + \mathbf{F} \cdot \frac{\partial f}{\partial \mathbf{c}} = \Omega = -\frac{1}{\tau}(f - f^{eq}), \quad (2.1)$$

where τ is the molecular collision relaxation time. The equilibrium velocity distribution $f^{eq}(\mathbf{r}, \mathbf{c}, t)$ in (2.1) is described by the Maxwell distribution,

$$f^{eq}(\mathbf{r}, \mathbf{c}, t) = n \left(\frac{1}{2\pi RT} \right)^{\frac{3}{2}} \exp \left(-\frac{(\mathbf{c} - \mathbf{u})^2}{2RT} \right). \quad (2.2)$$

In (2.2), $n(\mathbf{r}, t)$, $\mathbf{u}(\mathbf{r}, t)$ and $T(\mathbf{r}, t)$ are the macroscopic number density, mean velocity and temperature of the gas. They can be obtained by taking the first three moments of the distribution function:

$$\int f d^3 c = \int f^{eq} d^3 c = n, \quad (2.3a)$$

$$\int \mathbf{c} f d^3 c = \int \mathbf{c} f^{eq} d^3 c = n\mathbf{u}, \quad (2.3b)$$

$$\frac{1}{2} \int \mathbf{c}^2 f d^3 c = \frac{1}{2} \int \mathbf{c}^2 f^{eq} d^3 c = \frac{1}{2} n u^2 + n e, \quad (2.3c)$$

where e is the internal energy per unit volume which is related to the temperature by $e = 3RT/2$. It is noted that the last equalities in (2.3) are satisfied by $f^{eq}(\mathbf{r}, \mathbf{c}, t)$ automatically by definition and become the constraints to the efficiency in the discrete evaluation of the integrals (2.3).

3 Dynamic discrete ordinate method

3.1 Conventional discrete ordinate method

The analytical solution to the system of Eqs. (2.1)-(2.3) is very rare. Numerical procedure is a possible way to solve the equation system. Nevertheless, the number of dimension involved in the distribution function $f(\mathbf{r}, \mathbf{c}, t)$ prohibits from doing so. Conventionally, the discrete ordinate method (DOM) circumvents this difficulty by representing $f(\mathbf{r}, \mathbf{c}, t)$

with a set of the discrete distribution functions $f_i = f(\mathbf{r}, \mathbf{c}_i, t)$ at a discrete velocity \mathbf{c}_i , where i ($i = 1 - N$) is the index counting the number of the discrete velocities. The moments in (2.3) can then be approximated by summation over the index in a quadrature form. As a result, the equation system (2.1)-(2.3) becomes

$$\frac{\partial f_i}{\partial t} + \mathbf{c}_i \cdot \frac{\partial f_i}{\partial \mathbf{r}} + \mathbf{F} \cdot \frac{\partial f_i}{\partial \mathbf{c}_i} = -\frac{1}{\tau} (f_i - f_i^{eq}), \quad (3.1a)$$

$$f_i^{eq} = f^{eq}(\mathbf{r}, \mathbf{c}_i, t) = n \left(\frac{1}{2\pi RT} \right)^{\frac{3}{2}} \exp \left(-\frac{(\mathbf{c}_i - \mathbf{u})^2}{2RT} \right), \quad (3.1b)$$

with the three moments being written as,

$$\sum_i W_i f_i = n, \quad \sum_i W_i \mathbf{c}_i f_i = n\mathbf{u}, \quad \sum_i W_i (\mathbf{c}_i - \mathbf{u})^2 f_i = ne, \quad (3.2)$$

where W_i is the quadrature weighting coefficients of the moment integrals. The values of W_i can be determined by minimizing the errors incurred in

$$\sum_i W_i f_i^{eq} = n, \quad \sum_i W_i \mathbf{c}_i f_i^{eq} = n\mathbf{u}, \quad \sum_i W_i (\mathbf{c}_i - \mathbf{u})^2 f_i^{eq} = ne. \quad (3.3)$$

In the case of the conventional DOM, the Gaussian-Hermite quadrature is commonly employed because of the Gaussian-like behaviour of f_i^{eq} . The weighting coefficients W_i are then determined mathematically from the Gaussian-Hermite polynomials to provide high accurate results for (3.3). The discrete velocity set of \mathbf{c}_i is often obtained from the respective abscissas of this 1-D quadrature by expanding into higher dimensions.

From (3.1b), it is apparent that the errors incurred in (3.3) depend strongly on \mathbf{u} and T , which described the asymmetry and spreading of (3.1b), respectively. For high \mathbf{u} (i.e., high Mach number) and large variation in T , the set of fixed quadrature velocity \mathbf{c}_i will not be representative over the domain of computation. As a result, very large number of quadrature velocity set will be needed for gas flows at high Mach number. This renders the conventional DOM very impractical, particularly for 3-D flows.

3.2 Dynamic quadrature scheme

To circumvent the difficulty of high mean velocity (high Mach number) and large variation in temperature in the flow domain as described above, it is proposed to employ the following transformation,

$$\mathbf{C}^* = \frac{\mathbf{c} - \mathbf{u}}{\sqrt{2RT}}, \quad (3.4)$$

which represents basically the composition of a Galilean translation and a thermal normalization of \mathbf{c} . In term of \mathbf{C}^* , the equilibrium distribution (2.2) becomes

$$f^{eq}(\mathbf{r}, \mathbf{C}^*, t) = n \left(\frac{1}{2\pi RT} \right)^{\frac{3}{2}} \exp(-\mathbf{C}^{*2}). \quad (3.5)$$

Note that the shape of exponential in (3.5) is independent of \mathbf{u} and T . This independence facilitates the quadrature implementation. The moment integrals (2.3) now can be re-expressed in quadrature form as below,

$$\frac{1}{n} \int f^{eq}(\mathbf{r}, \mathbf{c}, t) d^3c = \pi^{-\frac{3}{2}} \int \exp(-C^{*2}) d^3C^* = \sum_i^N w_i F_i = 1, \quad (3.6a)$$

$$\frac{1}{n\sqrt{2RT}} \int (\mathbf{c} - \mathbf{u}) f^{eq}(\mathbf{r}, \mathbf{c}, t) d^3c = \pi^{-\frac{3}{2}} \int \mathbf{C}^* \exp(-C^{*2}) d^3C^* = \sum_i^N w_i \mathbf{C}_i^* F_i = 1, \quad (3.6b)$$

$$\frac{1}{4nRT} \int (\mathbf{c} - \mathbf{u})^2 f^{eq}(\mathbf{r}, \mathbf{c}, t) d^3c = \frac{1}{2} \pi^{-\frac{3}{2}} \int C^{*2} \exp(-C^{*2}) d^3C^* = \frac{1}{2} \sum_i^N w_i C_i^{*2} F_i = \frac{3}{4}, \quad (3.6c)$$

where $F_i = \pi^{-3/2}$. The quadrature points \mathbf{C}_i^* and the weightings w_i can be determined mathematically from the Gaussian-Hermite polynomial. In (3.6), a polynomial greater than 2 degree will result in zero error. The salient feature is that the quadrature points \mathbf{C}_i^* are fixed and independent of the mean velocity and temperature, i.e., independent of the Mach number of the gas flows.

In numerical evaluation, the hydrodynamic moments (3.2) can be computed by the following expression:

$$n = \sum_i J w_i f(\mathbf{r}, \mathbf{c}_i, t), \quad n\mathbf{u} = \sum_i J w_i \mathbf{c}_i f(\mathbf{r}, \mathbf{c}_i, t), \quad (3.7a)$$

$$ne = \frac{1}{2} \sum_i J w_i (\mathbf{c}_i - \mathbf{u})^2 f(\mathbf{r}, \mathbf{c}_i, t), \quad (3.7b)$$

where J is the Jacobian and

$$\mathbf{c}_i = a\mathbf{C}_i^* + \mathbf{u}$$

with fixed \mathbf{C}_i^* . Here, $a = \sqrt{2RT}$ is the characteristic velocity of sound propagation. For gas flows of small Knudson number, the error encountered in (3.7) is in the order of Knudson number as inferred from the Chapman-Enskog expansion. From $\mathbf{c}_i = a\mathbf{C}_i^* + \mathbf{u}$, the quadrature points \mathbf{c}_i will change from time-to-time and location-to-location in the physical space with fixed \mathbf{C}_i^* , and hence this scheme is termed as the Dynamic Quadrature Scheme (DQS). The discrete ordinate method with the DQS is then termed as the Dynamic Discrete Ordinate Method (DDOM). We noted that an expression similar to (3.4) had also been used by Albright et al. [14] and Smith et al. [15] to replace the random sample procedure for the reduction of the high numerical noise encountered in DSMC.

4 Dynamic lattice Boltzmann method

The LBM is a subset of DOM. It is the special case of DOM where the discrete velocities are specifically designed to ensure that particle leaves one node will end at other nodes.

In LBM, the fixed discrete velocity set is applied over the entire computation domain disregarding the orientation. Therefore it can only be applied efficiently to the velocity distributions which are isotropic and homogeneous. In currently-used (conventional) LBM, a set of fixed discrete velocity \mathbf{c}_i is usually adapted. To ensure the Gaussian symmetry with respect to \mathbf{c}_i , f^{eq} is conventionally expanded into power series under a small Mach number assumption and the series is truncated at certain order as needed. The truncation leads to errors which become significant when the Mach number increases. Also, the inhomogeneous problem incurred from the variations of u and T over the computation domain remains. For these reasons, the conventional LBM scheme has only been demonstrated to perform well-behaved for incompressible and isothermal flows, which defy the original physics of Boltzmann equation. Much effort has been devoted to the conventional LBM in the past decades to remove these incompressible and isothermal restrictions, but of less success. From the discussion in the last section, it appears that \mathbf{C}_i^* will be a better discrete velocity set for an LBM operation, since \mathbf{C}_i^* is independent of u and T and there is no need of power series expansion of f^{eq} . To this end, we transformed the Boltzmann equation through the following coordinate transformation,

$$d\mathbf{r}^* = \frac{d\mathbf{r}}{a\tau_0}, \quad \mathbf{C}^* = \frac{\mathbf{c} - \mathbf{u}}{a}, \quad dt^* = \frac{dt}{\tau_0}, \quad (4.1)$$

where τ_0 is a constant reference time. The Boltzmann equation in the new transformed coordinates $(\mathbf{r}^*, \mathbf{C}^*, t^*)$ now becomes

$$\frac{\partial f^*}{\partial t^*} + (\mathbf{C}^* + \mathbf{u}^*) \cdot \frac{\partial f^*}{\partial \mathbf{r}^*} + \mathbf{F}^* \cdot \frac{\partial f^*}{\partial \mathbf{C}^*} - \frac{\tau_0 Da}{a} \frac{D\mathbf{a}}{Dt} \mathbf{C}^* \cdot \frac{\partial f^*}{\partial \mathbf{C}^*} - \frac{\tau_0 D\mathbf{u}}{a} \frac{D\mathbf{u}}{Dt} \cdot \frac{\partial f^*}{\partial \mathbf{C}^*} = \Omega^*, \quad (4.2)$$

where $D/Dt = \partial/\partial t + \mathbf{c} \cdot (\partial/\partial \mathbf{r})$ is the Lagrangian derivative in the physical space, $f^* = f/n_0$, $\mathbf{u}^* = \mathbf{u}/a$, $\mathbf{F}^* = \mathbf{F}\tau_0/a$ and $\Omega^* = \Omega\tau_0/n_0$. Eq. (4.2) shows that the transformation leads to three additional terms associated with the convection due to \mathbf{u} and the accelerations due to \mathbf{u} and a , as compared to (2.1). The transformed equilibrium distribution is

$$f^{*eq} = n^* (\pi a^2)^{-\frac{3}{2}} \exp(-\mathbf{C}^{*2}), \quad (4.3)$$

where $n^* = n/n_0$. The moment integrals and constraints of the moments with respect to f^{eq} then become

$$\frac{a^3}{n^*} \int f^* d^3 C^* = \frac{a^3}{n^*} \int f^{*eq} d^3 C^* = 1, \quad (4.4a)$$

$$\frac{a^3}{n^*} \int \mathbf{C}^* f^* d^3 C^* = \frac{a^3}{n^*} \int \mathbf{C}^* f^{*eq} d^3 C^* = 0, \quad (4.4b)$$

$$\frac{a^3}{2n^*} \int C^{*2} f^* d^3 C^* = \frac{a^3}{2n^*} \int C^{*2} f^{*eq} d^3 C^* = \frac{3}{4}. \quad (4.4c)$$

Eqs. (4.2)-(4.4) can be solved with LBM in the transformed coordinates by considering the convection and acceleration terms as source terms. The equivalence between (3.6)

and (4.4) implies that no error may incur if a Gaussian-Hermite quadrature higher than 2 degree is employed to (4.4). As for DDOM, we call this new LBM with dynamic \mathbf{c}_i in physical space as Dynamic Lattice Boltzmann Method (DLBM).

5 Simplified DLBM for gas flows

The numerical procedure for the DLBM is a complicated procedure since it requires the Galilean translation in the \mathbf{c} space and the local coordinate stretching in both the \mathbf{c} and \mathbf{r} spaces. For thermal problems where the temperature variation is not so large, it is possible to simplify the procedure by employing Galilean translation only. This can be achieved by using a constant reference sound speed $a_0 = \sqrt{2RT_0}$ where T_0 is the reference temperature. Eq. (4.2) is then reduced to

$$\frac{\partial f^*}{\partial t^*} + (\mathbf{C}^* + \mathbf{u}^*) \cdot \frac{\partial f^*}{\partial \mathbf{r}^*} + \mathbf{F}^* \cdot \frac{\partial f^*}{\partial \mathbf{C}^*} - \frac{D\mathbf{u}^*}{Dt^*} \cdot \frac{\partial f^*}{\partial \mathbf{C}^*} = \Omega^*. \quad (5.1)$$

Eq. (5.1) is the same as the equation of change given in the book by Chapman and Cowling [16], who focused on the mean velocity transports to establish the NSF equations through the Chapman-Enskog expansion. Here we focus on the peculiar velocity, and consider the streaming process in the \mathbf{C}^* velocity space for the LBM simulation.

It is noted that this simplified DLBM is readily suitable for dealing with the problems of thermal flows with moderate temperature change and Mach number. When the physical particle velocity is not altered for more than $0.3a_0$, the results are satisfactory (the detailed results are to be reported in a later paper). If higher temperature variation is required, a larger discrete velocity set can always be employed to improve the accuracy by capturing temperature variations. But this kind of velocity set needs velocities and coefficients of different quadrature that will lose the salient features of Gaussian-Hermite quadrature, as the Gaussian-Hermite quadrature is only applicable up to 3 degree per dimension for LBM, i.e., D2Q9 for 2 dimensional flows or D3Q27 for a 3 dimensional flows.

6 Numerical results and validation

The DDOM has been validated for 1-D Sod problem, 2-D Riemann problem, and backward-step problem, and the DLBM has been validated for the thermal instability of Raleigh-Benard convection (RBC). The specifications of the physical problem and the results from the DDOM and DLBM simulations are discussed in the following subsections.

6.1 DDOM: One-dimensional Sod problem

There are different problems of one-dimensional Riemann shock tubes, depending on the initial conditions of the density, pressure and velocity. Here we use the Sod problem [18]

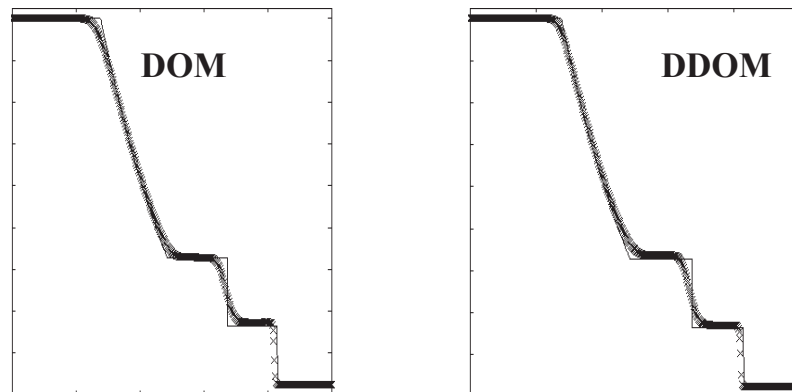


Figure 1: Density profiles of Sod test. The solid line is the exact solution.

as the bench mark for testing the one-dimensional DDOM against the conventional DOM. For the Sod problem, the velocity initially is zero, but with differences in density and pressure. For the present Sod test, the initial condition is:

$$(\rho, u, p) = \begin{cases} (1.0, 0.0, 1.0), & x \leq 0.5, \\ (0.125, 0.0, 0.1), & x > 0.5. \end{cases} \quad (6.1)$$

For this test, 400 grid points and $\Delta t / \Delta x = 0.376$ are used. Here, the 1-D DDOM simulation gives the results of Euler limit for inviscid flows.

Fig. 1 shows the results of density profiles at times $t = 0.188$ for the Sod problem. In Fig. 1, the dot lines represent the exact solutions. The small deviation of the numerical results from the exact solutions is typical for the current numerical scheme with numerical diffusivity. Although both DOM and DDOM provide the results agreeable to the exact solution, the computational efficiencies of the two are quite different. The DDOM is about 5 times faster than the DOM. This speed-up is basically in-line with the quadrature points needed for the simulations to reach the same accuracy. For the DDOM only 3 quadrature points are needed, while the number of quadrature points needed for conventional DOM is 18.

6.2 DDOM: Two-dimensional Riemann problem

The 2-D Riemann problem is defined in the x - y domain $(0,1) \times (0,1)$, which is divided by two lines $x = 0.5$ and $y = 0.5$ into four quadrants. The subscripts ll , lr , ul , and ur are used to denote lower-left, lower-right, upper-left and upper-right quadrants respectively. The initial data consists of a single constant state in each of the four quadrants. The configuration 8 of the 2-D Riemann problem is selected in this study as the benchmark

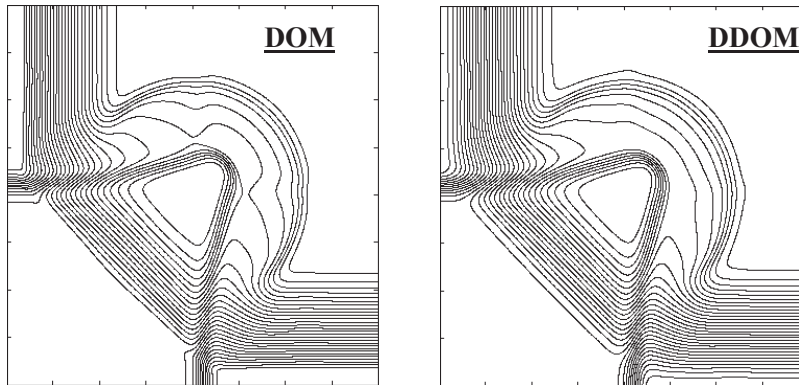


Figure 2: Density contour at $t=0.25$ for the configuration 8 of the 2D Riemann problem.

problem. The values of $V = (p, \rho, u, v)$ in the four quadrants as the initial conditions are:

$$\begin{cases} V_{ul} = (1.0, 1.0, 0.6259, 0.1), & V_{ur} = (0.4, 0.5197, 0.1, 0.1), \\ V_{ll} = (1.0, 0.8, 0.1, 0.1), & V_{lr} = (1.0, 1.0, 0.1, 0.6259). \end{cases} \quad (6.2)$$

For this test, the grid mesh is set at 400×400 with $\Delta t / \Delta x = 0.25$. Again, the simulation results represent those of Euler limit of inviscid flows.

Fig. 2 shows the contour of density at $t = 0.25$. It is seen that the density profiles and contour are well resolved both by DOM and DDOM. In order to obtain the results converging to the same degree of accuracy, 16 quadrature abscissas per each dimension are required for DOM, while only 2 quadrature abscissas are needed by DDOM. These demonstrate that DDOM provide much faster convergence rate than the conventional DOM. An efficiency of 20-times faster in computational time by DDOM than by conventional DOM can be achieved for this 2-D Riemann problem. Again, this is mainly due to the much less quadrature points are needed for DDOM than for DOM. Much higher efficiency in computational time can be expected for 3-D problems. Moreover, the convergence rate of DDOM scheme is insensitive to the mean velocity and temperature since the quadrature velocities for the DDOM is dimensionless.

6.3 DDOM: Two-dimensional backward-step problem

The backward step is constructed from a square and a rectangular region ranging from $(0,1) \times (0,1)$. The regions are separated by the step corner at $x = 0.5$ and $y = 0.5$. We will use the subscripts l and r to denote left and right regions respectively. The initial conditions for $V = (p, \rho, u, v)$ are:

$$\begin{cases} V_l = (2.4583, 1.862, 0.8216, 0), \\ V_r = (1, 1, 0, 0). \end{cases} \quad (6.3)$$

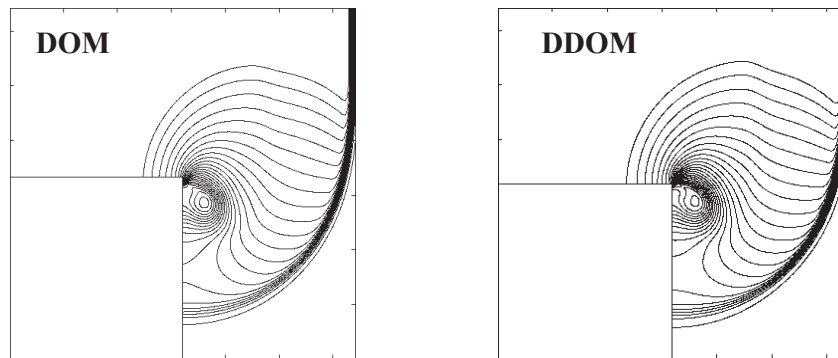


Figure 3: Density contours of 2-D backward step problem at Mach number 1.5 when $t=0.75$.

The contour map of density at $t = 0.75$ solved on a 320×320 mesh with $\Delta t / \Delta x = 0.2$ is shown in Fig. 3. Again, we found both DDOM and DOM schemes can yield the results in good agreement. For the same degree of accuracy, the number of quadrature points required for DOM is 18×18 , while only 3×3 is needed for DDOM. We found the speed-up ratio is 15 for this test.

6.4 DLBM: Thermal instability of Rayleigh-Benard convection

In the implementation of a 3-D numerical code to validate DLBM, we choose a D3Q27 lattice for the discretization of the phase space. The Gaussian-Hermite quadrature with the weighting coefficients determined from Gaussian-Hermite polynomial is adapted. The streaming and collision procedures in the DLBM are similar to those of conventional LBM. The acceleration and convection terms in Eq. (5.1) are discretized using central difference method. A Strang splitting algorithm is used to achieve a second-order Lagrangian streaming. The boundary conditions on the wall are typical diffused reflection as in some conventional LBM. The details of the numerical procedure can be found in [18–20].

Rayleigh-Benard convection (RBC) flows describe a viscous fluid at rest between two horizontal plates $z=0$ and $z=d$. There is a typical temperature difference ΔT between two plates with the lower plate at higher temperature, and the direction of gravity is towards negative z -direction. Due to the local thermal expansion effect, the lower fluid has less density and tends to buoy upwards, and the top heavier fluid tends to sink. This system is unstable when ΔT reaches a certain critical value. This type of flow instability is characterized by the non-dimensional parameter, Rayleigh number Ra , which is defined by $Ra = \beta g d^3 \Delta T / \nu \alpha$, where β is the volumetric thermal expansion coefficient, g the gravitational acceleration, d the separation between the two plates, ΔT the temperature difference, ν the kinematic viscosity, and α the thermal diffusivity. The critical Rayleigh number Ra_c varies for different regimes. At lower Ra_c the significant flow phenomenon is the 2 dimensional convective rolls. Through non-linear stability analysis, it can be found

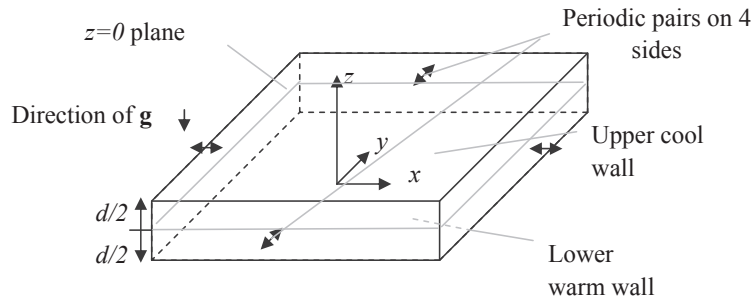


Figure 4: Schematic of computation domain: The origin of the coordinates is located at the center of the domain. The bottom wall is heated at constant temperature and the gravity is directed to the negative z direction. The four vertical sides are set as two periodic pairs.

that the critical Rayleigh number Ra_c is about 1708 [21], with the critical wave number $k_c^* = \pi d/w$ being around 3.117 where w is the wave length.

Fig. 4 shows the schematic of the computation domain with the coordinate system used in the present numerical simulation of the RBC flows. In Fig. 4, the origin is located at the center of the domain. Hence, $z=0$ is the mid-plane and $z = \pm d/2$ represent the top and bottom surfaces. Asymmetric boundary conditions at the top and bottom surfaces are set in the simulation. The heated bottom is at a fixed constant temperature T_{bottom} and the cooled top plate is under a relaxation condition to the desired ambient temperature, corresponding to a constant overall heat flux losing to the environment from the top surface. The four vertical boundaries are two pairs of periodic boundaries which are set consistently along each axis. Different mesh sizes are chosen for each problem.

Initially the velocity in the entire domain is zero and the fluid temperature equals to the cooled ambient temperature. For the simulation of the unstable flows of 2-D convective rolls, both horizontal walls are of no-slip boundary. For the 3-D RBC simulations, the cool top surface is a slip boundary and the hot bottom surface is a no-slip plate.

The connection between the NSF equation and Boltzmann equation can be established with the analysis based on the Chapman-Enskog expansion [16]. The NSF equation, when given an appropriate equation of state, can be reformulated into the equations with Boussinesq approximation, which is the set of equations often employed for studying natural convection problem. Since the equation of state is already embedded in the definitions of dynamic pressure and temperature of gases, the Boltzmann equation is its original form for solving the natural convection problem for gases. It is noted that Boussinesq approximation and fluid physical property modelling, which are usually used in macroscopic simulation of the RBC flows, are not required in our DLBM simulation.

For the simulation of the RBC flows with the convection rolls perpendicular to the x - z plane, a relatively short dimension in the y -direction is adapted and the periodic boundary in the lateral y -direction is enforced. The domain size is $137 \times 7 \times 23$. The grid size Δx employed for the DLBM is 0.02. A temperature difference of $\Delta T = 0.2$ is established between the top and bottom plates. Initially at $t = 0$, the fluid in the domain is stagnant

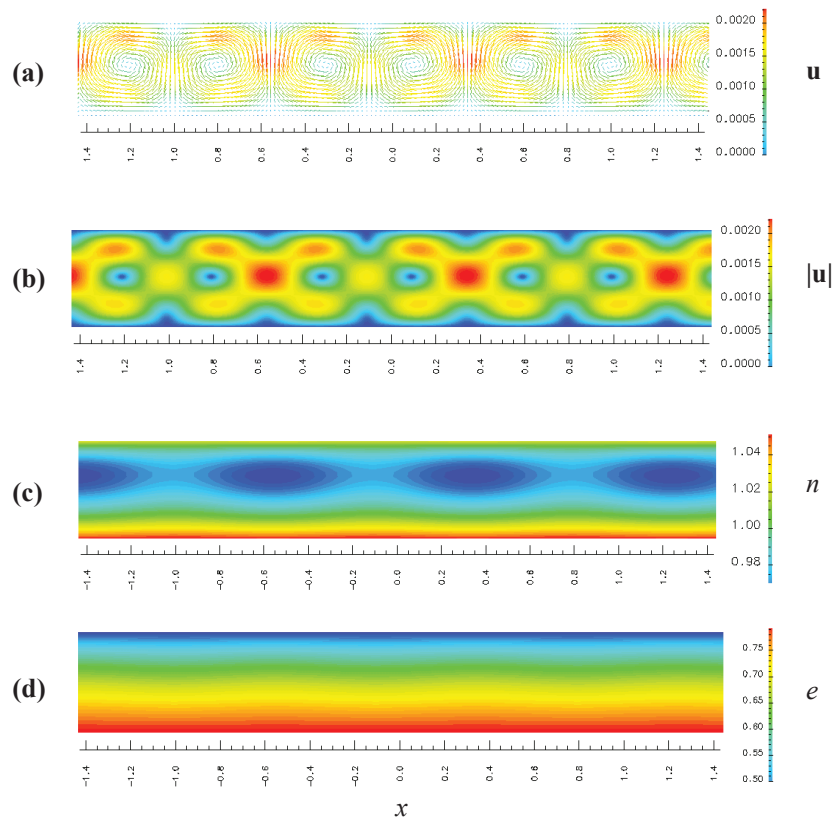


Figure 5: The simulation of 2-dimensional convective rolls using the 3-D DLBM code. The view is on the x - z plane. A periodic boundary condition is applied along the y direction.

and the gravitational acceleration \mathbf{g} is 0.01 towards negative z direction. Fig. 5 shows the colour-contoured distributions of (a) the mean velocity \mathbf{u} , (b) the velocity magnitude $|\mathbf{u}|$, (c) the number density n and (d) the temperature in term of e , as predicted by the 3-D DLBM code. For the present case, the Rayleigh number is $Ra = 1600$, and the wave number obtained from the present simulation is approximately 3.1, which is close to the theoretical value. From Figs. 5(a) and (b), it is seen that the maximum velocities of down-flow and up-flow at $z = 0$ are asymmetric. The velocity magnitude of up-flow is higher than that of the down-flow. As a result, the centers of vortex circulation are shifted toward the down-flow regions. Hence, the down-flow regions become narrower than the up-flow regions. Apparently, this asymmetry is the consequence of the buoyancy force which is aligned with the temperature gradient in the negative gravitational direction. The gas fluids in the up-flow regions are accelerated by the buoyancy force while those in the down-flow regions are decelerated. This is also in conformal to the gas density distribution represented by n as shown in Fig. 5(c), where the minimal density region is in-line with the up-flow region. Fig. 5(c) also shows the occurrence of density stratifica-

tion with high density near the bottom wall. This density stratification may be the consequence of the gravitational potential. The temperature distribution given in Fig. 5(d) shows basically a constant thermal gradient in the z -direction, hardly of seeing a periodic temperature perturbation.

To simulate the 3-D RBC flow structure, the computational domain is set as $103 \times 103 \times 23$ for the case of hexagonal cell and $123 \times 123 \times 23$ for the case of convective rolls. The simulation parameters are similar to those of the 2-D RBC case, except that Δx is changed to 0.04, and that the gravitational force is doubled to 0.02. The top boundary is applied with a slip flow boundary condition, and the temperature is maintained at a mean value of a simple relaxation in time. The flow field is allowed to evolve for 10^5 time steps until the resultant flow evolves very slowly at a change in mean velocity less than 10^{-4} of the nominal value. Two Rayleigh numbers at $Ra = 1800$ and 4000 were used in the present 3-D DLBM simulation.

The results of the simulated RBC flows are shown in Fig. 6, for the case of $Ra = 4000$ when the periodic hexagonal cells occur (Figs. 6(a1)-(a3)) and for the case of $Ra = 1800$ when the convective vortex rolls occur (Figs. 6(b1)-(b3)). Figs. 6(a1) and (b1) show the distributions of mean speed at the top surface ($z = d/2$) where the boundary condition is set to be slippery. The motion of gas flows in the red region is in parallel to the x - y top plane, and that in the blue regions is normal to the plane. Hence, in Fig. 6(a1), the gas flows move upward from the external region of the hexagons, pass over the red-band strip and then move downward into the central inner region of the hexagons. For the vortex rolls shown in Fig. 6(b1), the gas flows move upward from one blue strip, pass over the red strip and then move downward at the next blue region. As being inferred from the asymmetry of the up and down motions in the convective rolls as described above, the wider blue strip represents the up-flow region while the narrower blue strip represents the down-flow region. The occurrence of the oblique convective rolls as shown in Fig. 6(b1) is common when the ranges of computation domain in the x and y directions are of the same order. Figs. 6(a2) and (b2) of the temperature distributions indicate that the up-flow regions are wider and hotter than the down-flow regions. On the horizontal x - y plane at $z=0$, the gas flows have almost no horizontal motions on the plane, i.e., only the z -component of the velocity w survives. The distributions of the w velocity component for the gas flows with hexagon cells and convective rolls are shown in Figs. 6(a3) and (b3), respectively. Clearly, in Fig. 6(a3) the up-flow regions are shown by the red positive w region external to the hexagon cells, and in Fig. 6(b3) by the red strips of the convective rolls.

From the above results, it is clearly that the new DLBM is capable to accurately simulate the behaviours of the thermal instability of Rayleigh-Benard convection (RBC) using the DQS with D3Q27. To our knowledge to date, such simulation of RBC in 3-D has never been achieved by a conventional LBM using a simple Boltzmann equation. The success of the DLBM in simulating the RBC is attributed to the use of DQS that, with the proper coordinate transformation, has basically removed the incompressible and isothermal restrictions encountered by the conventional LBM.

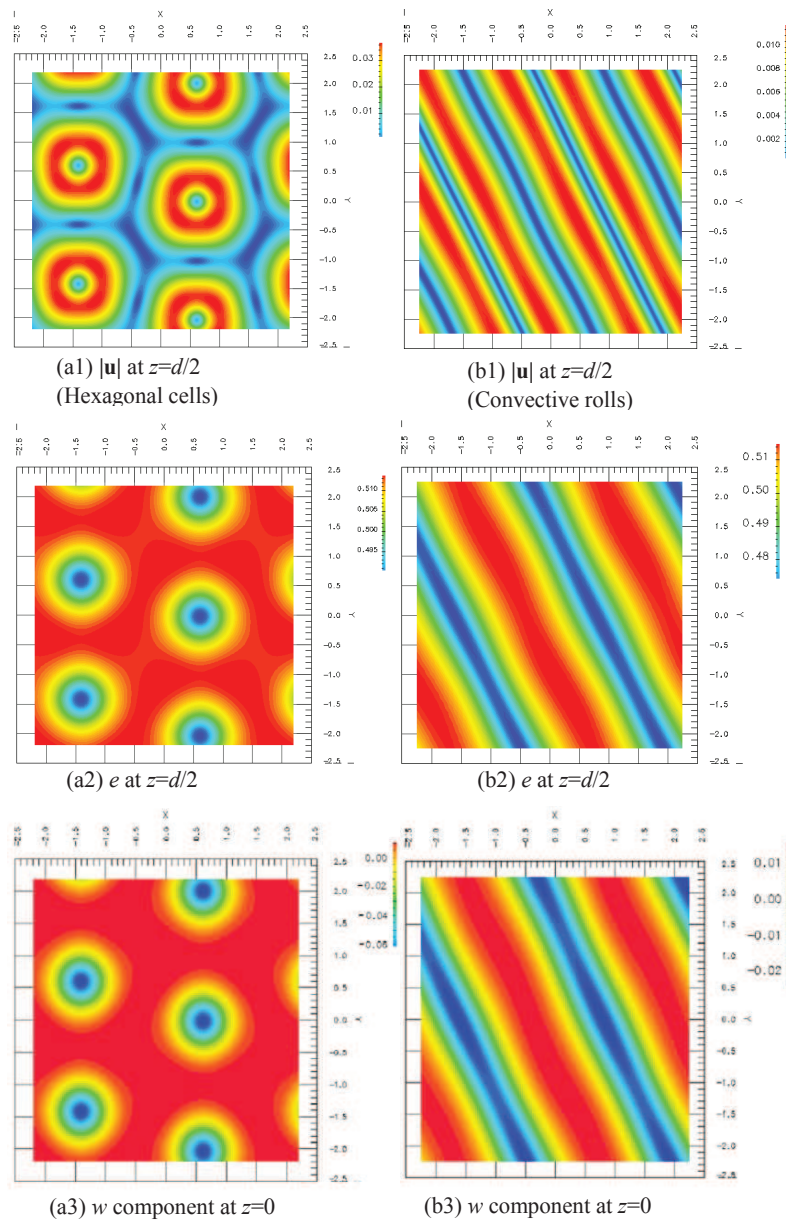


Figure 6: The simulation results of 3-D Rayleigh-Benard convection. The hexagonal cells (a1)-(a3) occur at $Ra=4000$, and the convective rolls (b1)-(b3) occur at $Ra=1800$.

7 Conclusions

In this paper, a dynamics quadrature scheme (DQS) is proposed to evaluate the moment integrals very accurately in the formulation of Boltzmann equation for gas flows.

This is accomplished by the transformation of the physical velocity-space into a non-dimensional velocity-space through a Galilean translation and a thermal normalization. With such transformation, the shape of Maxwellian equilibrium distribution is fixed and symmetry. Therefore, the first three moments of the equilibrium distribution can be calculated exactly with zero errors using 3 quadrature points in each dimension, i.e., using D1Q3, D2Q9, and D3Q27 for the discrete velocities. The salient feature of the DQS is its independence of the mean velocity and temperature. With the dynamic nature of quadrature velocities in physical space, the Dynamic Discrete Ordinate Methods (DDOM) and the Dynamic Lattice Boltzmann Method (DLBM) are formulated, designed and simulated.

The DDOM was validated with the benchmark of 1-D Sod problem, 2-D Riemann problem and 2-D backward-step problem. Comparison of the DDOM solutions with those of conventional DOM shows excellent agreements. At the same degree of numerical accuracy, the efficiency in computational time at a factor of 20-times faster by DDOM than by conventional DOM has been achieved for the 2-D simulation. This speed-up is mainly due to the much less quadrature points needed for DDOM than for the conventional DOM, i.e., only 3 points is needed for DDOM while 18 points is required for conventional DOM. As the number of quadrature points for DDOM is insensitive to the mean velocity and temperature, it is anticipated that the speed-up will be much faster at higher Mach number. By this nature that only small number of fixed quadrature points is needed for DDOM, it is conceived that the DDOM has basically circumvented the difficulties of large quadrature points faced by the conventional DOM. It is anticipated that a speed gain of more than 100 times as compared to the conventional DOM simulations can be achieved for 3-D DDOM simulations. This DDOM has been evaluated in details [22] and extended to viscous flow problem [23].

The DLBM have been validated by the thermal instability problem of Rayleigh-Benard convection (RBC). Without the macroscopic modelling such as Boussinesq approximation, the 3-D DLBM simulations based on Boltzmann formulation have predicted the RBC flows that evolve naturally to patterns of 2-D vortex rolls at $Ra = 1800$ and of 3-D hexagonal cells at $Ra = 4000$. The results from DLBM are in excellent agreement with the experimental results from open literatures. To our knowledge, this prediction of 3-D RBC flows has never been achieved by the conventional LBM using a simple Boltzmann equation. The success of the DLBM in predicting RBC may be attributed to the implementation of DQS, which is insensitive to mean velocity and temperature variation. The use of DQS also leads to the isotropic behaviour of Maxwellian distribution in the transformed velocity-space, which is consistent with the spirit of a lattice method. Because no small Mach number expansion is required and the velocity is normalized with the thermal velocity in the DLBM, it is conceived that the new DLBM has basically removed the incompressible and isothermal restrictions encountered by the conventional LBM. As an important note, the new DLBM has basically retained the physics of gas flows in accordance to the original formulation of Boltzmann equation.

Acknowledgments

This work is supported by the ITC of Hong Kong Government through ITF under Contract No. GHP/028/08SZ.

References

- [1] J. E. Broadwell, Shock structure in a simple discrete velocity gas, *Phys. Fluids*, 7(8) (1964), 1243–1247.
- [2] J. E. Broadwell, Study of rarefied shear flow by the discrete velocity method, *J. Fluid Mech.*, 19(3) (1964), 401–414.
- [3] M. Krook, On the solution of equation of transfer I, *Astrophys. J.*, 122 (1955), 488–497.
- [4] L.-S. Luo, Some recent results on discrete velocity models and ramifications for lattice Boltzmann equation, *Comput. Phys. Commun.*, 129 (2000), 63–74.
- [5] J. Y. Yang and J. C. Huang, Rarefied flow computations using nonlinear model Boltzmann equations, *J. Comput. Phys.*, 120 (1995), 323–339.
- [6] J. Tjon and T. T. Wu, Numerical aspects of the approach to a Maxwellian distribution, *Phys. Rev. A*, 19(2) (1978), 883–888.
- [7] R. Benzi, S. Succi and M. Vergassola, The lattice Boltzmann equation: theory and applications, *Phys. Rep.*, 222(3) (1992), 145–197.
- [8] H. Chen, S. Chen and W. H. Matthaeus, Recovery of the Navier-Stokes equations using a lattice-gas Boltzmann method, *Phys. Rev. A*, 45(8) (1992), R5339.
- [9] S. Succi, *The Lattice Boltzmann Equation for Fluid Dynamics and Beyond*, Oxford, Clarendon Press, 2001.
- [10] G. R. McNamara and G. Zanetti, Use of the Boltzmann equation to simulate lattice-gas automata, *Phys. Rev. Lett.*, 61(20) (1988), 2332–2335.
- [11] S. Succi, A. A. Mohammad and J. Horbach, Lattice-Boltzmann simulation of dense nanoflows: a comparison with molecular dynamics and Navier-Stokes solutions, *Int. J. Mod. Phys. C*, 18(4) (2007), 667–675.
- [12] P. Lallemand and L. S. Luo, Theory of the lattice Boltzmann method: acoustic and thermal properties in two and three dimensions, *Phys. Rev. E*, 68(3) (2003), 3670601–3670625.
- [13] G. Karniadakis, A. Beskok and N. Aluru, *Microflows and Nanoflows: Fundamentals and Simulation*, New York, Springer, 2007.
- [14] B. J. Albright, D. S. Lemons, M. E. Jones and D. Winske, Quiet direct simulation of Eulerian fluid, *Phys. Rev. E*, 65 (2002), 055302.
- [15] M. R. Smith, H. M. Cave, J. S. Wu, M. C. Jermy and Y. S. Chen, An improved quiet direct simulation method for Eulerian fluids using a second-order scheme, *J. Comput. Phys.*, 228 (2009), 2213–2224.
- [16] S. Chapman and T. G. Cowling, *The Mathematical Theory of Non-Uniform Gases*, 3rd ed, Cambridge University Press, Cambridge, 1970.
- [17] G. A. Sod, Survey of several finite difference methods for systems of nonlinear hyperbolic conservation laws, *J. Comput. Phys.*, 27 (1978), 1–31.
- [18] C. T. Hsu, S. W. Chiang and K. F. Sin, Dynamic lattice Boltzmann method for the simulation of cavity flows with high performance computing, 22nd International Conference on Parallel Computational Fluid Dynamics, Kaohsiung, Taiwan, 2010.

- [19] K. F. Sin, S. W. Chiang and C. T. Hsu, Evaluation of dynamic discrete ordinate method for Boltzmann equation, The 8th Asian Computational Fluid Dynamics Conference, Hong Kong, 2010.
- [20] S. W. Chiang, K. F. Sin and C. T. Hsu, Numerical simulation of Rayleigh-Benard instability using dynamic lattice Boltzmann method, The 8th Asian Computational Fluid Dynamics Conference, 10-14 January 2010, Hong Kong, 2010.
- [21] P. G. Drazin, Introduction to Hydrodynamic Stability, Cambridge, Cambridge University Press, 2002.
- [22] C. T. Hsu, K. F. Sin and S. W. Chiang, Parallel computation for Boltzmann equation simulation with Dynamic Discrete Ordinate Method (DDOM), Computers and Physics, (2011), (in press).
- [23] C. T. Hsu, K. F. Sin and S. W. Chiang, Dynamic discrete ordinate method for Boltzmann equation in viscous flow, The 21st International Symposium on Transport Phenomena, November 2010, Taiwan, 2010.